Supporting Information

For

[2Fe-2S] Clusters Supported by *N*-Heterocyclic Carbene Ligands

Yuwei Ye,[a,b] Xuebin Jiang,[c,d] Qing Liu,[a,b] Shengfa Ye,[c,e*] Liang Deng[a,b*]

[a] School of Chemistry and Materials Science, Hangzhou Institute for Advanced Study, University of Chinese Academy of Sciences, 1 Sub-lane Xiangshan, Hangzhou 310024, P. R. China

[b] State Key Laboratory of Organometallic Chemistry, Shanghai Institute of Organic Chemistry, Chinese Academy of Sciences. 345 Lingling Road, Shanghai 200032, P. R. China

[c] State Key Laboratory of Catalysis, Dalian Institute of Chemical Physics, Chinese Academy of Sciences, Dalian 116023, China

[d] University of Chinese Academy of Sciences, Beijing 100049, China

[e] Key Laboratory of Bioinorganic and Synthetic Chemistry of Ministry of Education, Guangdong Basic Research Center of Excellence for Functional Molecular Engineering, School of Chemistry, IGCME, Sun Yat-sen University, Guangzhou 510275, China

Emails: deng@sioc.ac.cn; yeshf6@mail.sysu.edu.cn

Table of Contents

Experimental Section

General Procedures. All manipulations on air- and moisture-sensitive materials were performed under an atmosphere of dry dinitrogen with the rigid exclusion of air and moisture using standard Schlenk techniques, or in a glovebox. Solvents were dried with a solvent purification system (Innovative Technology) and degassed prior to use. $[(ICy)_2Fe(\eta^2-CH_2=CHSiMe_3)]$,[1] $[Cp_2Fe][BPh_4]$,[2] $[(IMes)Fe(\eta^2:\eta^2-dvtms)]$,[3] $[(Me_2-cAAC)Fe(\eta^2:\eta^2-dvtms)]$,[3] $IMes$[4] and I^iPr[5] were synthesized according to literature procedures. All other chemicals were purchased from chemical vendors and used as received unless otherwise noted. ^1H and ^{11}B spectra were recorded with BRUKER 400 MHz NMR spectrometer. All chemical shifts were reported in units of ppm with references to the residual protons of the deuterated solvents for proton chemical shifts, the ^{11}B of $BF_3 \cdot C_2H_5OC_2H_5$ for boron chemical shifts. $\nu_{1/2}$ is the peak width at the half-height of a signal. Elemental analyses were performed by the Analytical Laboratory of Shanghai Institute of Organic Chemistry (CAS). Solution magnetic moment was measured at room temperature by the method originally described by Evans with stock and experimental solutions containing a known amount of a $(CH_3)_3SiOSi(CH_3)_3$ standard.[6-7] Absorption spectra were recorded with a Shimadzu UV-3600 UV-vis-NIR spectrophotometer. Direct current (dc) susceptibility experiments were performed on Quantum Design MPMS XL-5 SQUID magnetometer on polycrystalline sample. All procedures were carried in the nitrogen gas filled glove box or under inert atmosphere. About 20 to 40 mg complexes were weighted and then put onto a thin parafilm and packaged. The sample was pressed into the white capsule to avoid the movement during the measurement. A small amount of N grease was used to protect the sample from the oxygen and moisture. IR spectra were recorded with a NICOLET AVATAR 330 FT-IR spectrophotometer.

Electrochemistry. Electrochemical measurements were carried out in a glovebox under an argon atmosphere with a CHI 600D potentiostation. A glassy carbon was used as working electrode; a platinum wire was used as the auxiliary electrode, and an SCE was used as reference electrode. 0.1 M $[(n-Bu)_4N][PF_6]$ in THF was used as supporting electrolyte and was prepared in the glovebox. Under these conditions, $E_{1/2} = 0.55$ V for the $[Cp_2Fe]^{0,+}$ couple.

Zero-field ^{57}Fe Mössbauer spectroscopy. Mössbauer spectra were recorded in an alternating constant WissEl Mössbauer spectrometer, which consists of an MR 360 drive unit, an MVT 1000 velocity transducer, and an KETEK AXAS-M Si-drifting detector mounted on an MB-500 Mössbauer bench with cryostat stand. The system was operated in a horizontal transmission geometry with source, absorber and detector in a linear arrangement. The γ-source (57Co/Rh, 0.925 GBq) was operated with alternating constant acceleration and kept at room temperature. The minimum experimental line width was 0.24 mm/s (full width at half maximum). The temperature was controlled and maintained using MBBC-N20106 Mössbauer cryostat produced by Cryo Industries of American Inc for liquid nitrogen connected with Lake Shore-325 temperature controller unit. Measurements were performed at 80K. Data acquisition was performed using a 512 channel analyzer. Isomer shifts are quoted relative to alpha-iron metal foil at 300 K. The zero-field spectra were simulated with Lorentzian doublets with the program mf.SL developed by Dr. Eckhard Bill at the MPI CEC. (Max-Planck Institute for Chemical Energy Conversion, Mülheim, Germany).

X-band EPR spectroscopy. Continuous-wave (cw) X-band EPR measurements were performed on a Bruker A200 spectrometer equipped with a high sensitivity cavity (ER4119HS) in conjunction with microwave bridge Bruker A40X. For variable temperature control, cryostat (A4131VT) was employed. EPR simulations have been carried out with esim due to Dr. Eckhard Bill at Max-Planck-Institut für Chemische Energiekonversion and Easyspin program.[8]

Magnetic Susceptibility Measurements. Magnetic susceptibility was obtained from powder samples immobilized in n-octadecane in the temperature range 2−300 K with a SQUID magnetometer at an applied field of 1 T (MPMS-7, Quantum Design; calibrated with a standard palladium reference sample; error <2%). Susceptibility data is plotted as χT vs T curves. Simulation of the experimental magnetic data was performed with the *julX* program: E. Bill, Max-Planck Institute for Chemical Energy Conversion, Mülheim/Ruhr, Germany.[9] The simulation of exchanging coupling constant is depended on Heisenberg-Dirac-van Vleck (HDvV) Hamiltonian functor $\hat{H}_{HDvV} = -2J\hat{S}_A \cdot \hat{S}_B$.

X-ray Structure Determination. Crystals of **1** and **2** were coated with Paratone-*N* oil and mounted on a Bruker D8 Venture diffractometer equipped with an Oxford low-temperature apparatus. Cell parameters were retrieved with SMART software and refined using SAINT software on all reflections. Data integration was performed with SAINT, which corrects for Lorentz-polarization and decay. Absorption corrections were applied using SADABS.[10] Space groups were assigned unambiguously by analysis of symmetry and systematic absences determined by XPREP.[11] All structures were solved and refined using OLEX 2.[12] The metal and first coordination sphere atoms were located from direct-methods *E* maps. Non-hydrogen atoms were found in alternating difference Fourier synthesis and least-squares refinement cycles and during the final cycles were refined anisotropically. CCDC 2388893, 2388894 contain the supplementary crystallographic data for **1** and **2**. These data can be obtained free of charge from The Cambridge Crystallographic Data Centre via www.ccdc.cam.ac.uk/data_request/cif.

Computational Details. All calculations were carried out by version 5.0.1 of the ORCA[13-14] program package using the broken-symmetry (BS) approach to approximate the multireference electronic states of Fe–S clusters. The structural optimization, estimations for ^{57}Fe Mössbauer parameters and exchange-coupling constant, as well as the calculations for spin density and unrestricted natural orbitals (UNOs) were all performed at B3LYP[15-16] level. For Fe and S atoms, the DKH-def2-TZVP[17] basis set was used; for C, N and H atoms, the DKH-def2-SVP[18] basis set was used. For all calculations, the DKH2 relativistic correction and the general-purpose Coulomb fitting basis set SARC/J[19] were used; all basis sets were fully decontracted. Calculations were accelerated through the use of the RIJCOSX[20] approximation with a fine auxiliary integration grid (GridX7). The Becke-Johnson damping scheme D3BJ has been used to utilize the atom-pairwise dispersion correction.[21-22] The molecular structures of **1** and **2** obtained from single-crystal X-ray diffraction studies were used for SCF calculations with only the positions of hydrogen atoms being optimized. For the calculation of Mössbauer parameters, CP(PPP)[23] basis set was used for Fe atoms and the isomer shift value was obtained by $\delta = \alpha(\rho\text{-C})+\beta$ formula[24]. The value of exchange-coupling constant was determined by $J = (E_{[HS]}-E_{[BS]})/(<\hat{S}^2>_{HS}-<\hat{S}^2>_{BS}))$[25-26].

Table S1. Crystal Data and Summary of Data Collection and Refinement for **1** and **2**.

	1	2
temperature	173 K	173 K
Formula	$C_{60}H_{96}Fe_2N_8S_2$	$C_{84}H_{116}BFe_2N_8S_2$
crystal size(mm^3)	$0.08 \times 0.08 \times 0.05$	$0.17 \times 0.07 \times 0.05$
Fw	1105.26	1424.47
crystal system	monoclinic	monoclinic
space group	C2/c	P2$_1$/c
a, Å	18.2092(5)	24.6146(4)
b, Å	23.0253(6)	13.8721(2)
c, Å	17.5429(4)	27.6794(5)
α, deg	90	90
β, deg.	93.991(2)	116.2260(10)
γ, deg.	90	90
V, Å^3	7337.4(3)	8478.4(2)
Z	4	4
D$_{calcd}$, Mg/m^3	1.001	1.116
radiation(λ), Å	GaKα (λ = 1.34139)	GaKα (λ = 1.34139)
2θ range, deg	5.392 to 110.088	6.35 to 110.056
μ, mm^{-1}	2.718	2.418
F(000)	2384	3060
no. of obsd reflns	35615	102247
no. of param refnd	6973	16114
Goodness of fit	1.110	1.053
[a]R$_1$[I>2sigma(I)]	0.0543	0.0392
[b]wR$_2$[I>2sigma(I)]	0.1688	0.1088

[a]$R_1 = \Sigma[(F_o - F_c)] / \Sigma(F_o)$. [b]$wR_2 = \{\Sigma[w(F_o^2 - F_c^2)^2 / \Sigma[w(F_o^2)^2]]^{1/2}$.

Preparation procedure and characterization data of [Fe$_2$(μ-S)$_2$(ICy)$_4$] (1).

To a stirring Et$_2$O (15 mL) solution of [(ICy)$_2$Fe(η^2-CH$_2$=CHSiMe$_3$)] (712 mg, 1.14 mmol) was added triphenylphosphine sulfide (335 mg, 1.14 mmol) at room temperature. The color of the solution changed from green to brown slowly. After further stirring for 6 h, the volatiles were removed under vacuum to yield yellowish brown solid that was washed with cold *n*-hexane (2 mL) and then dried under vacuum to give [Fe$_2$(μ-S)$_2$(ICy)$_4$] (1) as a yellowish brown powder (430 mg, 68%). Single-crystals of 1 were obtained by standing its saturated Et$_2$O solution at −30 °C for two days. ^{1}H NMR (400 MHz, C$_6$D$_6$, 295 K) δ (ppm) 9.32 ($v_{1/2}$ = 165.6 Hz), 4.62 ($v_{1/2}$ = 436.5 Hz), 2.84 ($v_{1/2}$ = 56.9 Hz), 2.39 ($v_{1/2}$ = 50.1 Hz), 1.69 ($v_{1/2}$ = 31.2 Hz), 1.28 ($v_{1/2}$ = 32.7 Hz). Solution magnetic susceptibility (C$_6$D$_6$, 295 K): μ_{eff} = 2.4 μB. Anal. Absorption spectrum (THF, 295 K): λ_{max} (ε) = 375 nm (7050 M^{-1}cm^{-1}), 437 nm (4200 M^{-1}cm^{-1}), 466 nm (3500 M^{-1}cm^{-1}) and 1200 nm (310 M^{-1}cm^{-1}). Calcd for C$_{60}$H$_{96}$Fe$_2$N$_8$S$_2$: C, 65.20; H, 8.75; N, 10.14. Found: C, 65.29; H, 8.67; N, 10.04.
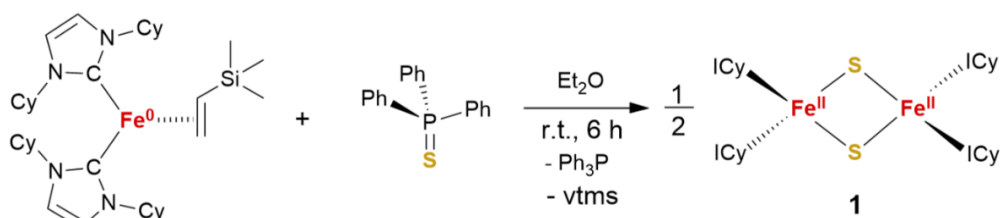
Scheme S1. Synthesis of [Fe$_2$(μ-S)$_2$(ICy)$_4$] (1).

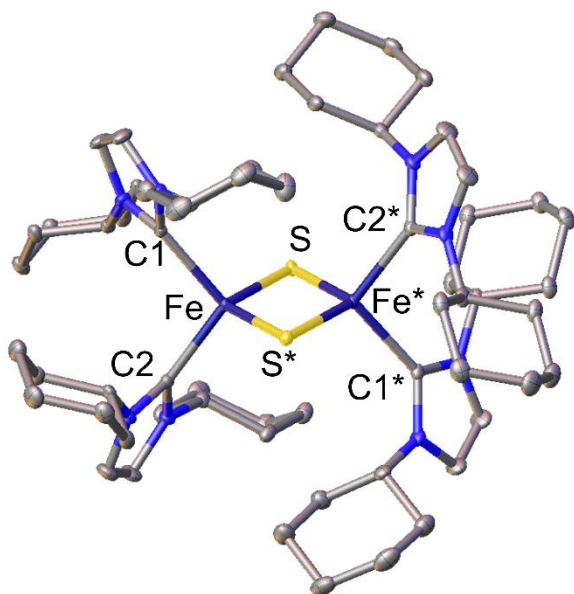**Figure S1.** Molecular structure of $[Fe_2(\mu\text{-}S)_2(ICy)_4]$ (**1**) showing 50% probability ellipsoids and the partial atom numbering scheme. All hydrogen atoms were omitted for clarity. Selected distances (Å) and angles (deg): Fe-Fe* 2.6655(7), Fe-S 2.2479(8), Fe-S* 2.2482(8), Fe-C(1) 2.099(3), Fe-C(2) 2.087(3), S-Fe-S* 107.28(2), Fe-S-Fe* 72.72(3), Fe-S*-Fe* 72.71(3).
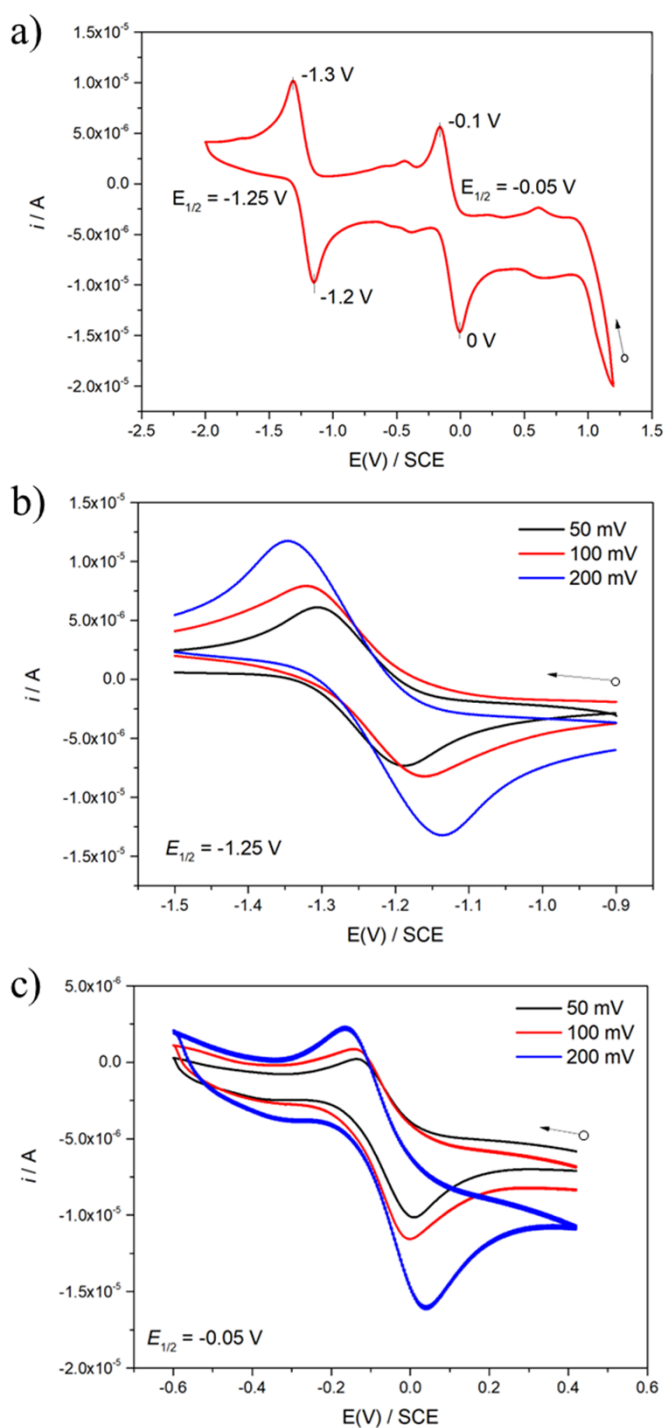
Figure S2. a) Cyclic voltammogram (200 mV/s) of $[Fe_2(\mu\text{-}S)_2(ICy)_4]$ (**1**) in THF with 0.10 M $[Bu^n_4N][PF_6]$ supporting electrolyte; b) voltammogram (50 mV/s, 100 mV/s and 200 mV/s) at -0.8 to -1.6 V; c) voltammogram (50 mV/s, 100 mV/s and 200 mV/s) at -0.6 to 0.6 V. Number peak potentials *vs.* SCE are indicated.
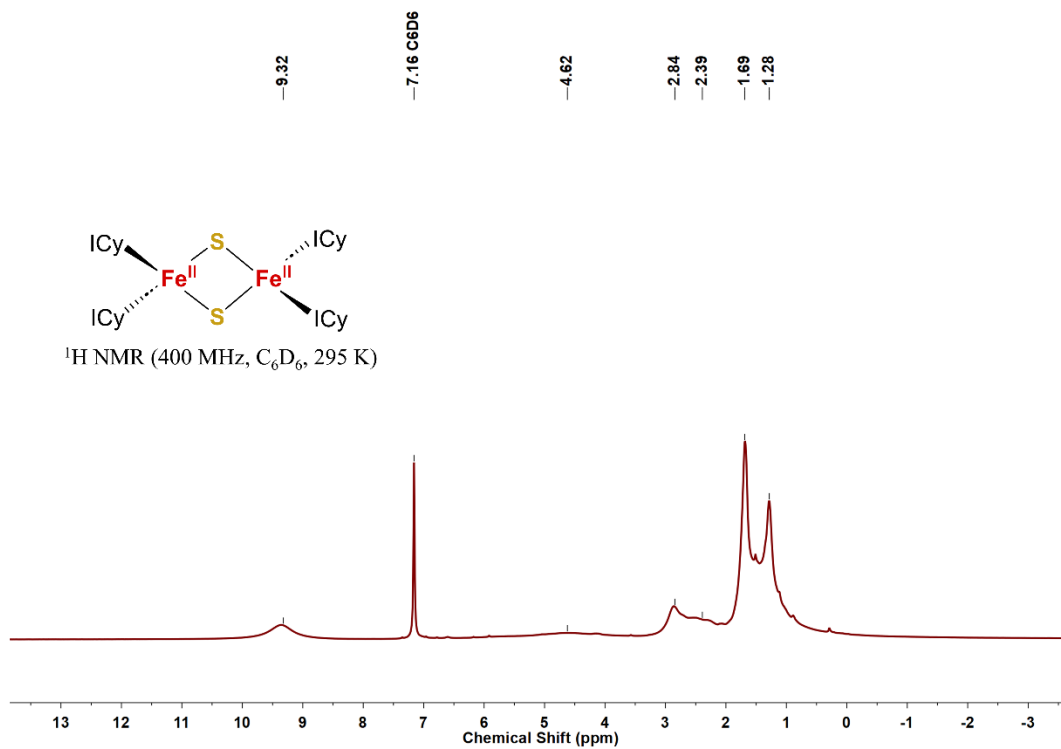
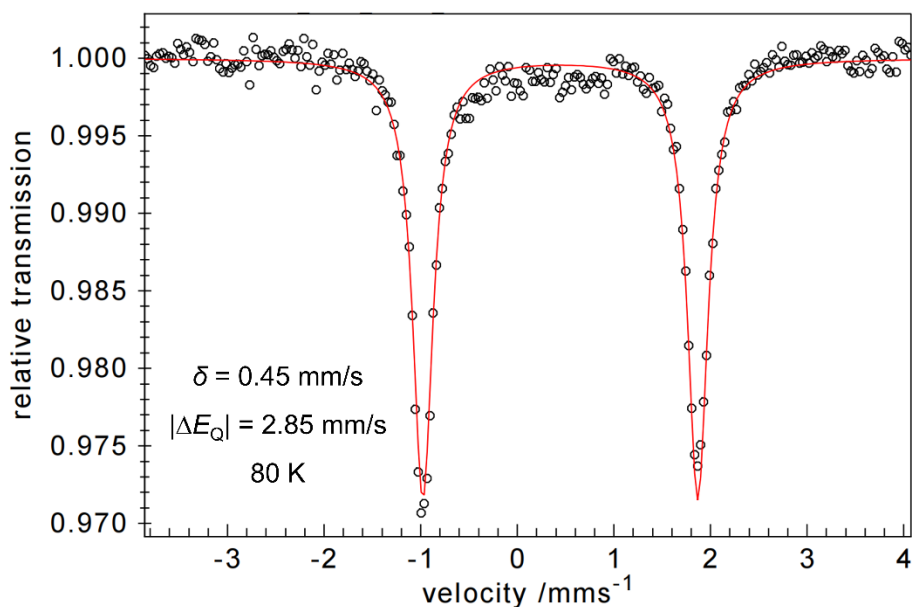**Figure S3.** ^{1}H NMR spectrum of [Fe$_2$(μ-S)$_2$(ICy)$_4$] (**1**) in C$_6$D$_6$ (400 MHz, 295 K).

Figure S4. Zero-field ^{57}Fe Mössbauer spectrum of $[Fe_2(\mu\text{-}S)_2(ICy)_4]$ (**1**) measured at 80 K. The following parameters have been fitted to the experimental values: $\delta = 0.45$ mm/s, $|\Delta E_Q| = 2.85$ mm/s.
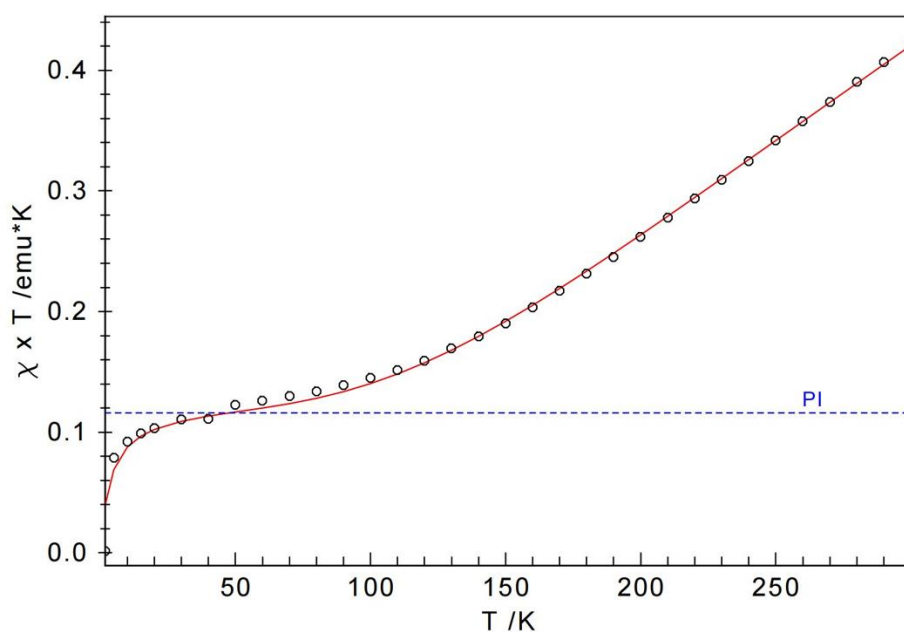

Figure S5. Variable temperature magnetic susceptibility data for $[Fe_2(\mu\text{-}S)_2(ICy)_4]$ (**1**) collected under a 1 kOe applied dc field. The red solid line is fitted to the experimental values (circles), taking a paramagnetic impurity PI ($S = 2$) into account (blue dotted line). Best fit parameters: $J = -208$ cm^{-1}, $PI = 3.9\%$, $D_1 = D_2 = -80$ cm^{-1}, $(E/D)_1 = (E/D)_2 = 0.08$, $g_1 = g_2 = 2.000$ (fixed).
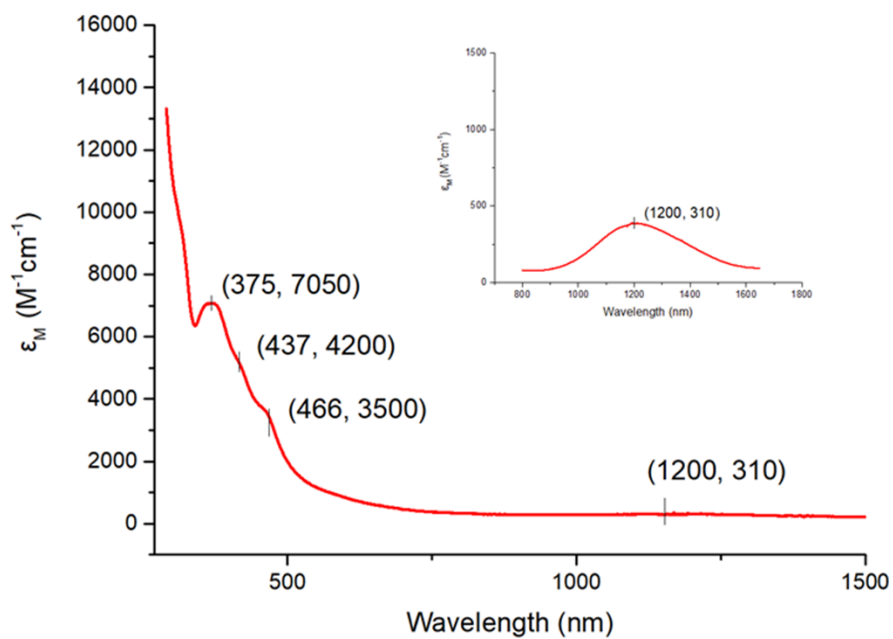
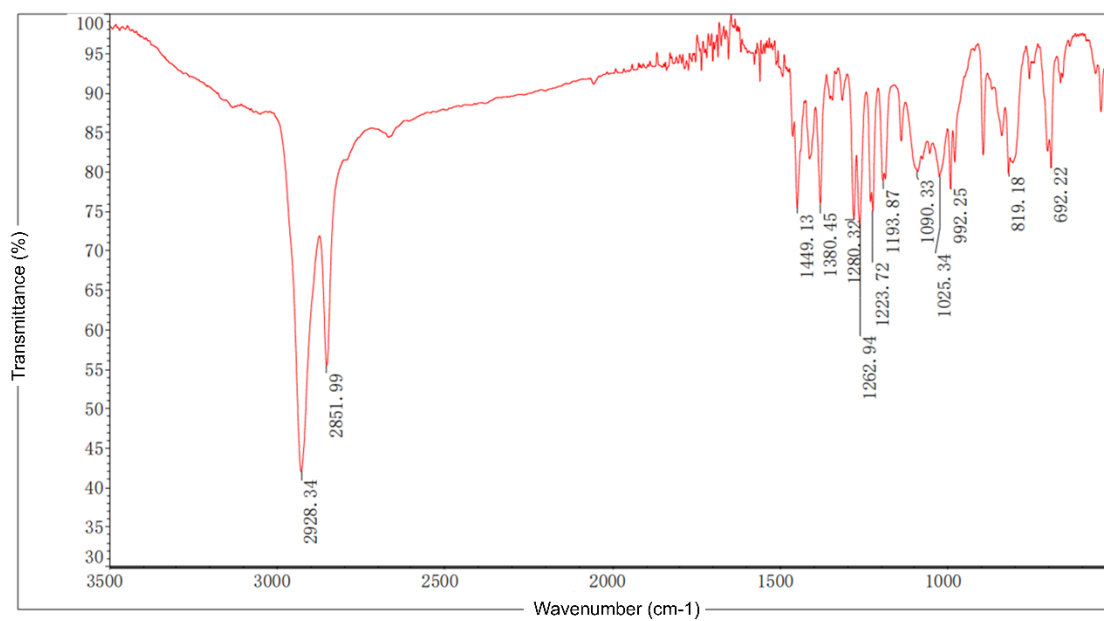**Figure S6.** Absorption spectrum of [Fe$_2$(μ-S)$_2$(ICy)$_4$] (**1**) measured at room temperature in THF.

Figure S7. IR spectrum for [Fe$_2$(μ-S)$_2$(ICy)$_4$] (**1**).
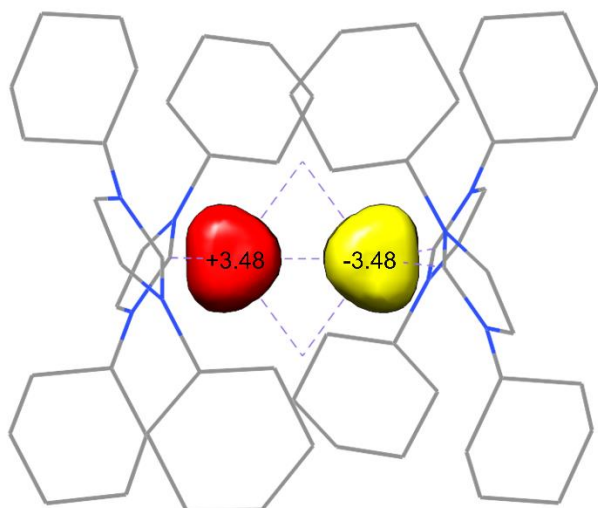
Figure S8. Mulliken spin density population of [Fe$_2$(μ-S)$_2$(ICy)$_4$] (**1**) for the $S = 0$ state.

Orbital	UNO 292	UNO 293	UNO 294	UNO 295	UNO 296
Occupation Number	1.99	1.98	1.40	1.25	1.14

Orbital	UNO 297	UNO 298	UNO 299	UNO 300	UNO 301
Occupation Number	1.02	0.98	0.86	0.75	0.60

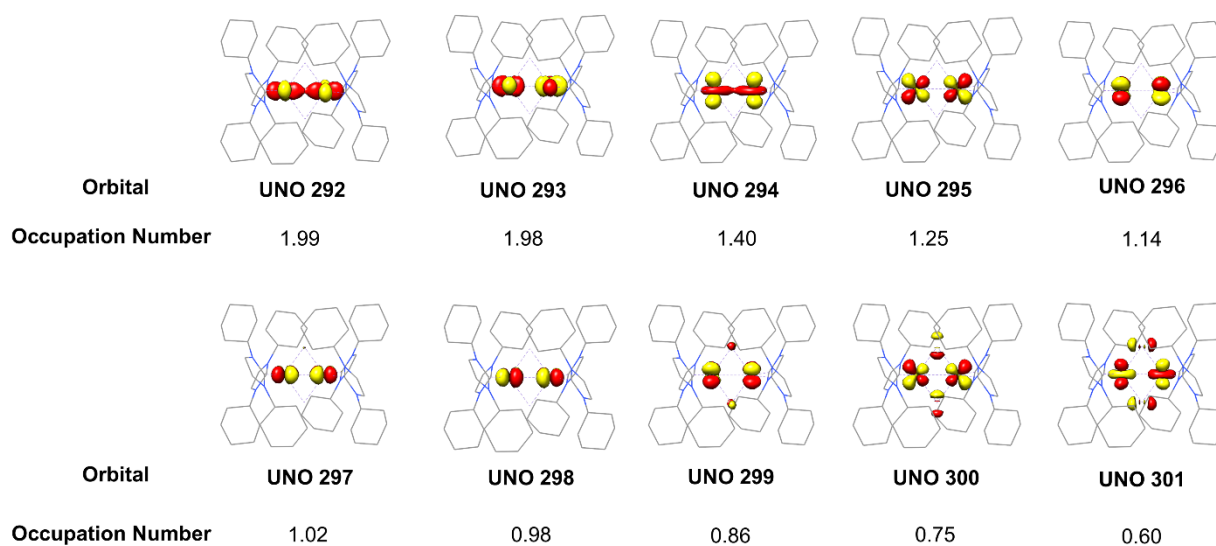**Figure S9.** Selected unrestricted natural orbitals (UNOs) of [Fe$_2$(μ-S)$_2$(ICy)$_4$] (**1**) in the antiferromagnetic spin state ($S = 0$).

UCO 297α
Fe1 $3d$ 73.9%
S1 $2p$ 3.5%
S2 $2p$ 2.3%

$S_{\alpha\beta} = 0.02$

UCO 297β
Fe2 $3d$ 73.9%
S1 $2p$ 3.5%
S2 $2p$ 2.3%

UCO 296α
Fe1 $3d$ 87.4%
Fe2 $3d$ 2.3%
S1 $2p$ 2.4%
S2 $2p$ 3.2%

$S_{\alpha\beta} = 0.19$

UCO 296β
Fe1 $3d$ 2.3%
Fe2 $3d$ 87.3%
S1 $2p$ 2.4%
S2 $2p$ 3.2%

UCO 295α
Fe1 $3d$ 73%
Fe2 $3d$ 5.5%
S1 $2p$ 4.6%
S2 $2p$ 4.5%

$S_{\alpha\beta} = 0.36$

UCO 295β
Fe1 $3d$ 5.5%
Fe2 $3d$ 73%
S1 $2p$ 4.6%
S2 $2p$ 4.5%

UCO 294α
Fe1 $3d$ 73.5%
Fe2 $3d$ 10.7%
S1 $2p$ 3.2%
S2 $2p$ 2.2%

$S_{\alpha\beta} = 0.53$

UCO 294β
Fe1 $3d$ 10.7%
Fe2 $3d$ 73.5%
S1 $2p$ 3.2%
S2 $2p$ 2.2%

UNO 293
Fe1 $3d$ 44.5%
Fe2 $3d$ 44.5%
S1 $2p$ 1.3%
S2 $2p$ 1.5%

UNO 292
Fe1 $3d$ 44.3%
Fe2 $3d$ 44.4%

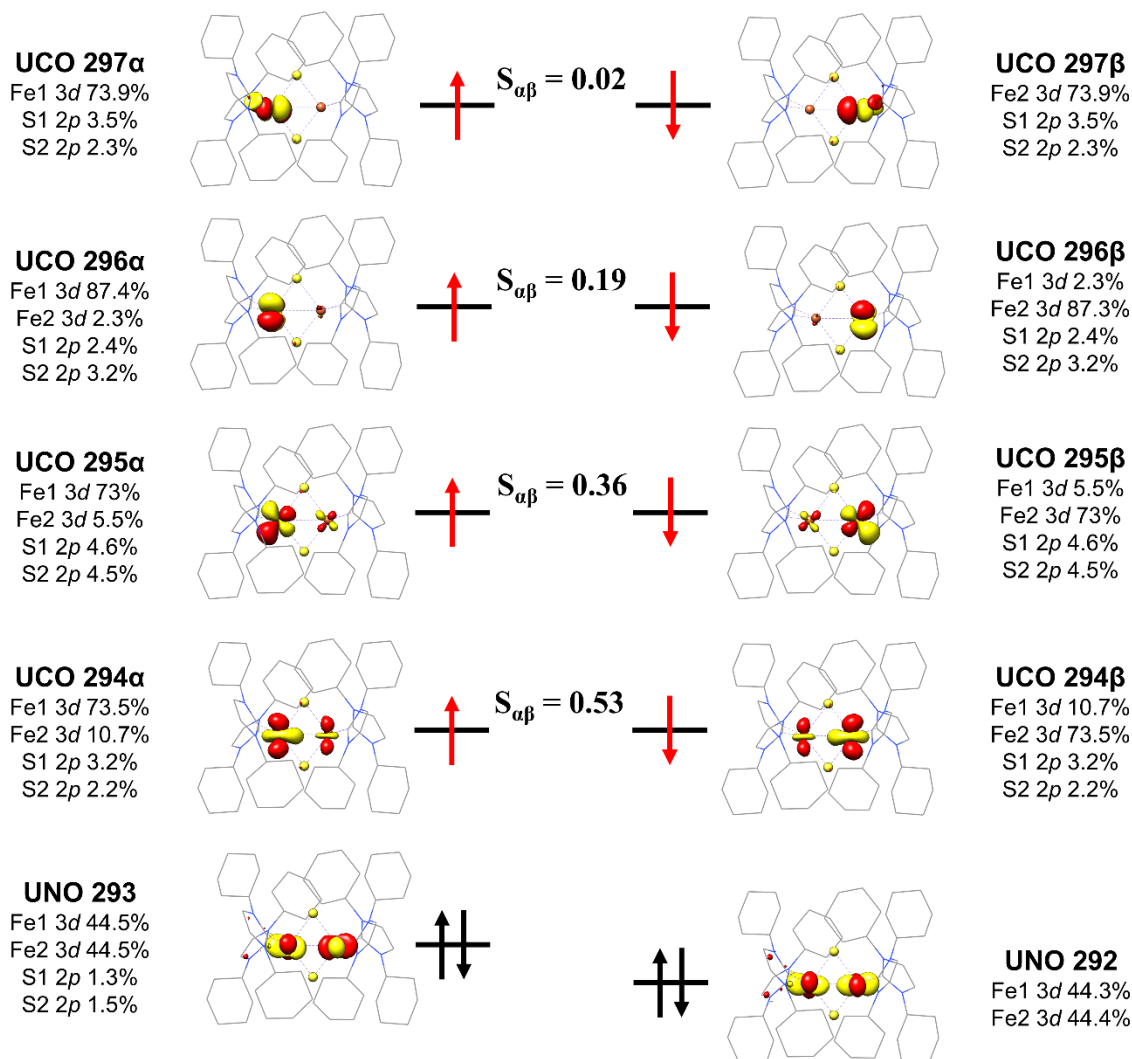**Figure S10.** Selected unrestricted natural orbitals (UNOs) and unrestricted corresponding orbitals (UCOs) of [Fe$_2$(μ-S)$_2$(ICy)$_4$] (**1**) in the antiferromagnetic spin state ($S = 0$).

Preparation procedure and characterization data of [Fe$_2$(μ-S)$_2$(ICy)$_4$][BPh$_4$] (2).

To a THF (10 mL) solution of [Fe$_2$(μ-S)$_2$(ICy)$_4$] (160 mg, 0.14 mmol) in a 25 mL flask was added [Cp$_2$Fe][BPh$_4$] (76 mg, 0.14 mmol) at room temperature. The solution quickly changed from yellowish brown to reddish brown. After stirring for 30 min, the solution was subjected to vacuum to remove the solvent. The resultant residue was washed with *n*-hexane (5 mL) to remove Cp$_2$Fe. The residue was dried under vacuum to afford [Fe$_2$(μ-S)$_2$(ICy)$_4$][BPh$_4$] (**2**) as a red powder (190 mg, yield: 92%). ^{1}H NMR (400 MHz, THF-d_8, 298 K) δ (ppm) 8.81 ($\nu_{1/2}$ = 29.5 Hz), 7.31 (s, 8H), 6.85 (s, 8H), 6.71 (s, 4H), 4.11 ($\nu_{1/2}$ = 32.9 Hz), 3.07 ($\nu_{1/2}$ = 121.4 Hz), 2.04 ($\nu_{1/2}$ = 62.4 Hz), 1.43 ($\nu_{1/2}$ = 59.5 Hz). ^{11}B NMR (128 MHz, THF-d_8, 298 K) δ (ppm) -6.51. Solution magnetic susceptibility (THF-d_8, 298 K): μ_{eff} = 2.6(1) μB. Absorption spectrum (THF, 298 K): λ_{max} (ε) = 355 nm (6430 M^{-1}cm^{-1}), 447 nm (2670 M^{-1}cm^{-1}) and 546 nm (870 M^{-1}cm^{-1}). Anal. Calcd for C$_{84}$H$_{116}$BFe$_2$N$_8$S$_2$: C, 70.83; H, 8.21; N, 7.87. Found: C, 70.25; H, 8.38; N, 7.73.
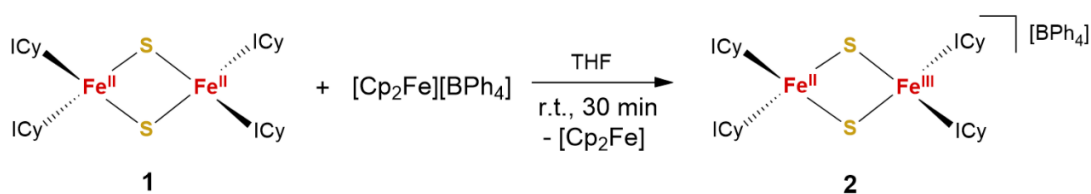
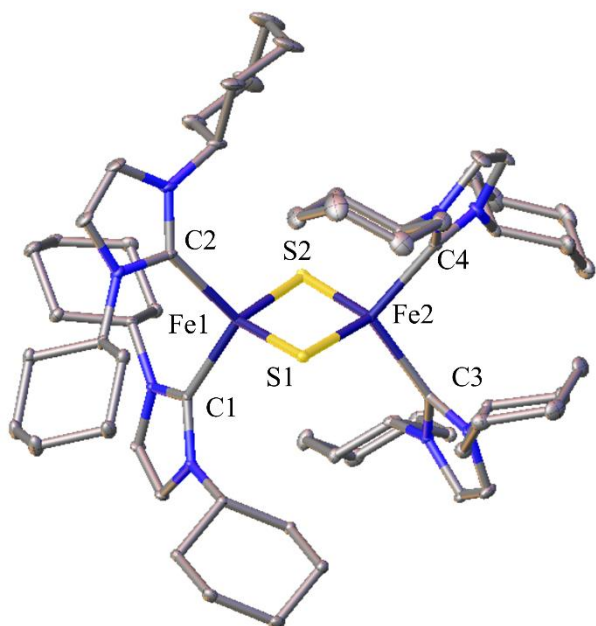**Scheme S2**. Synthesis of [Fe$_2$(μ-S)$_2$(ICy)$_4$][BPh$_4$] (**2**).

Figure S11. Structure of the cation in [Fe$_2$(μ-S)$_2$(ICy)$_4$][BPh$_4$] (**2**) showing 50% probability ellipsoids and the partial atom numbering scheme. The anion [BPh$_4$]$^-$ and all hydrogen atoms were omitted for clarity. Selected distances (Å) and angles (deg): Fe(1)-Fe(2) 2.6814(4), Fe(1)-S(1) 2.1888(5), Fe(1)-S(2) 2.2069(5), Fe(1)-C(1) 2.1268(17), Fe(1)-C(2) 2.1116(19), Fe(2)-S(1) 2.2232(5), Fe(2)-S(2) 2.2245(5), Fe(2)-C3 2.1106(18), Fe(2)-C(4) 2.0948(19), S(1)-Fe(1)-S(2) 106.161(19), Fe(1)-S(1)-Fe(2) 74.847(16), Fe(1)-S(2)-Fe(2) 74.467(16)).
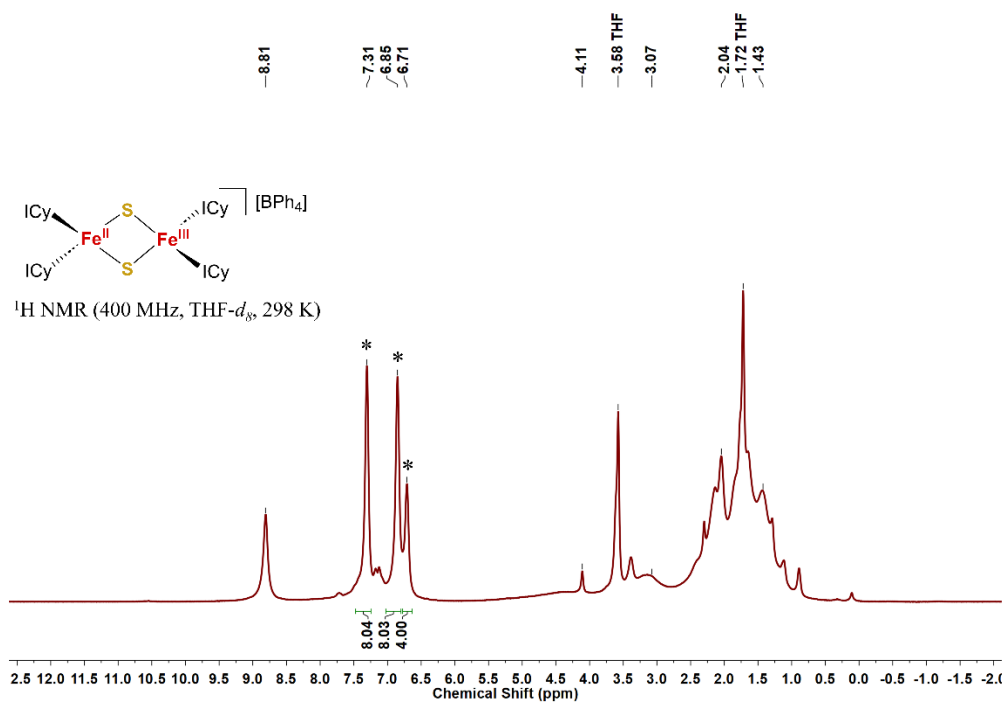
Figure S12. ^{1}H NMR spectrum of [Fe$_2$(μ-S)$_2$(ICy)$_4$][BPh$_4$] (**2**) in THF-d_8 (400 MHz, 298 K). * denotes signals for [BPh$_4$]$^-$.
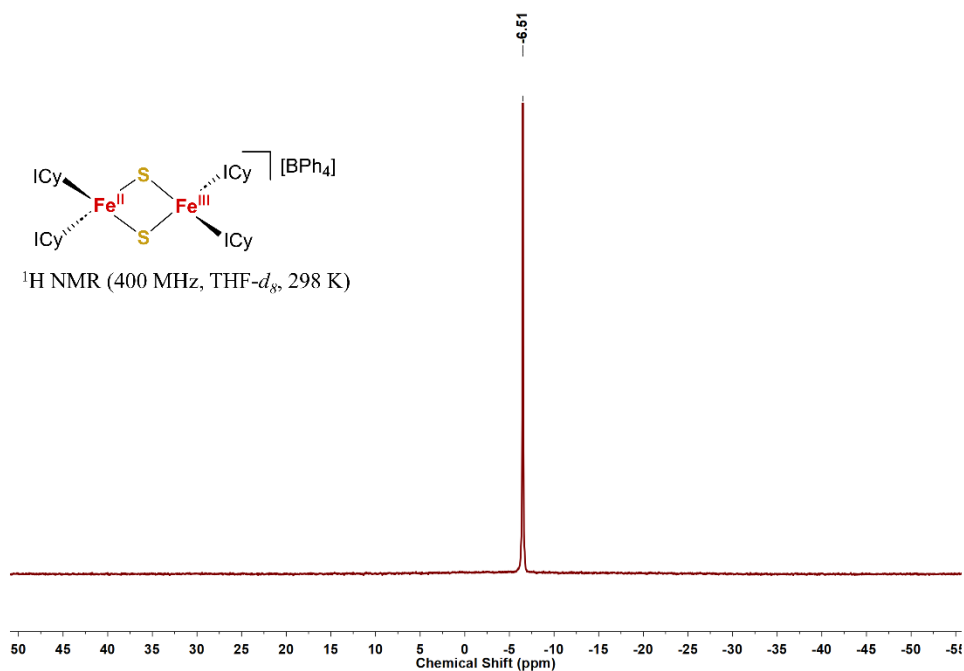
Figure S13. ^{11}B NMR spectrum of [Fe$_2$(μ-S)$_2$(ICy)$_4$][BPh$_4$] (**2**) in THF-d_8 (128 MHz, 298 K).
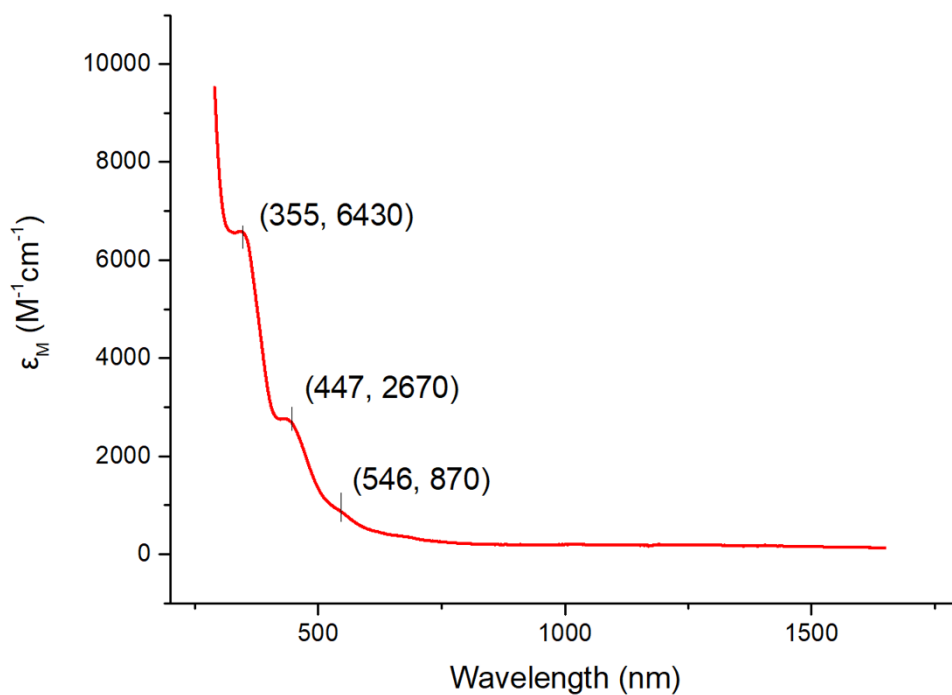
Figure S14. Absorption spectrum of [Fe$_2$(μ-S)$_2$(ICy)$_4$][BPh$_4$] (**2**) measured at room temperature in THF.
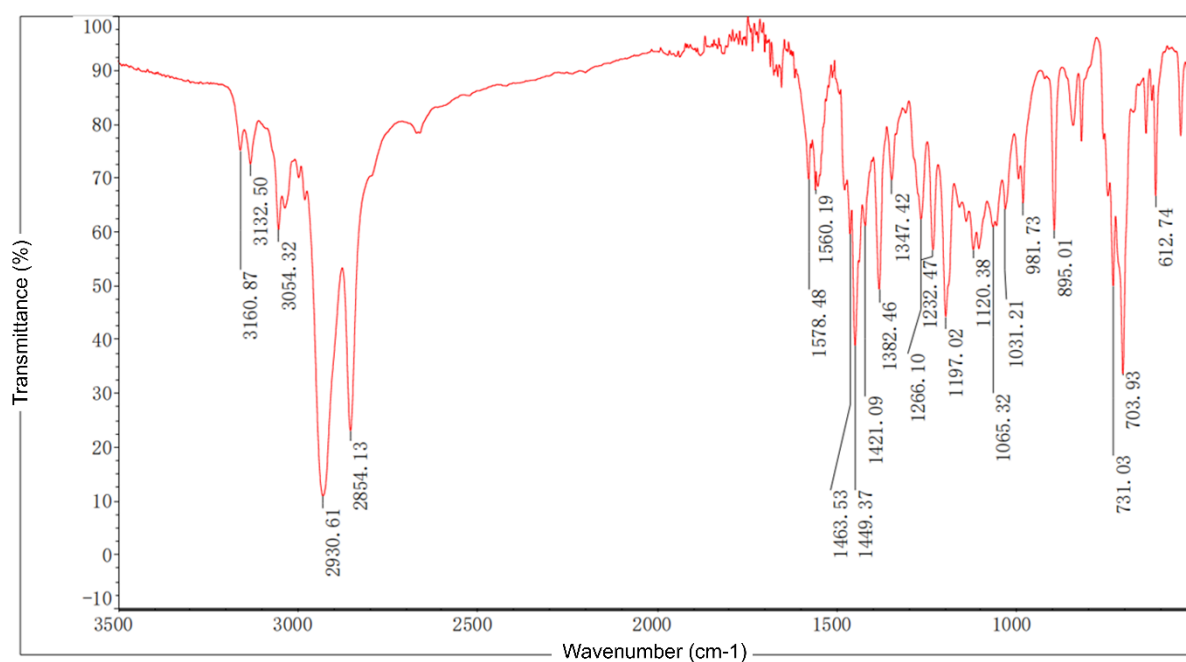
Figure S15. IR spectrum for [Fe$_2$(μ-S)$_2$(ICy)$_4$][BPh$_4$] (**2**).
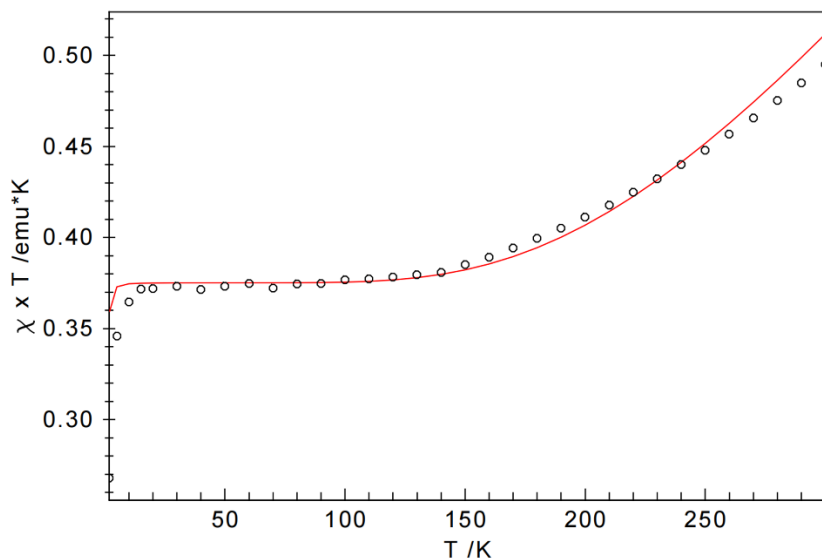
Figure S16. Variable temperature magnetic susceptibility data for $[Fe_2(\mu\text{-}S)_2(ICy)_4][BPh_4]$ (**2**) collected under a 1 kOe applied dc field. Best fit parameters: $J = -210$ cm^{-1}, $\chi(TIP) = 1260 \times 10^{-6}$ emu (subtracted), $g_1 = g_2 = 2.000$ (fixed).

Figure S17. EPR spectrum of $[Fe_2(\mu\text{-}S)_2(ICy)_4][BPh_4]$ (**2**) recorded at 123 K in frozen 2-MeTHF solution. The red line is a powder simulation with $g = (1.986, 1.945, 1.934)$.

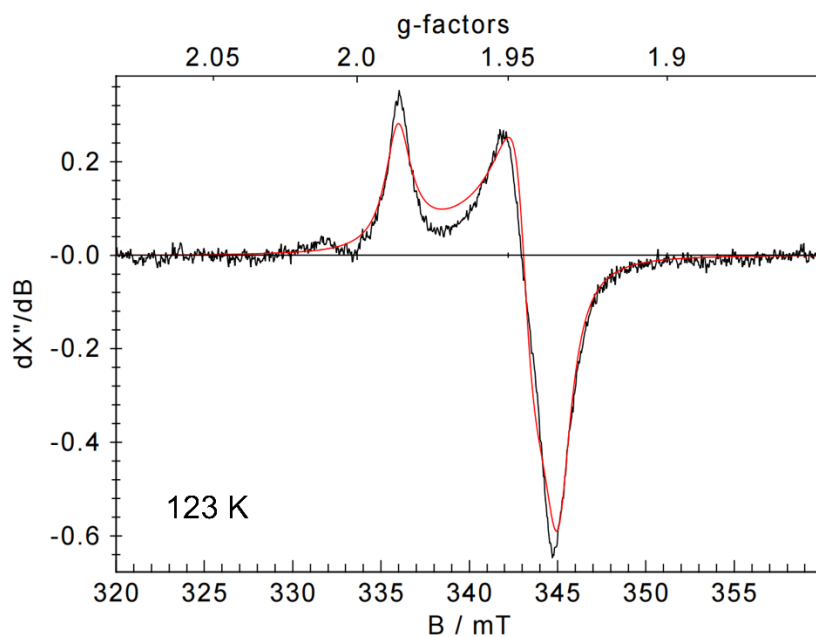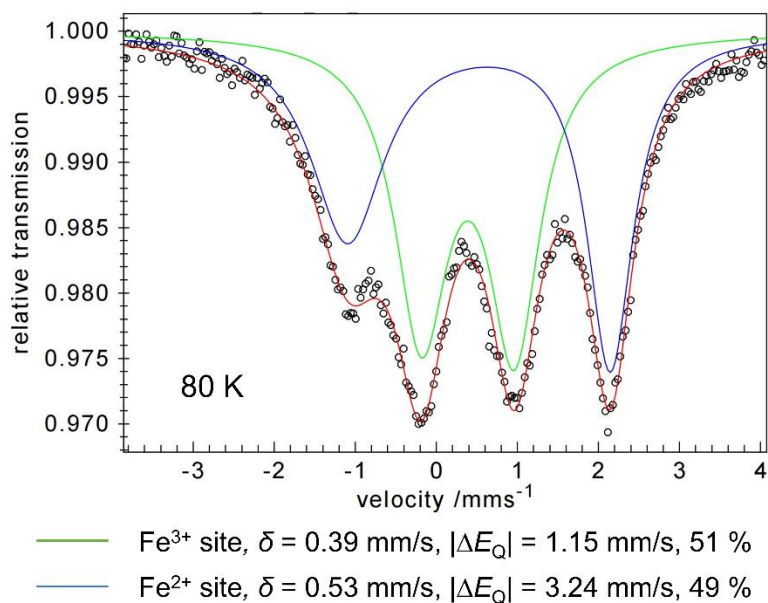**Figure S18.** Zero-field ^{57}Fe Mössbauer spectrum of [Fe$_2$(μ-S)$_2$(ICy)$_4$][BPh$_4$] (**2**) measured at 80 K. Green and blue sub-spectra are fitted to the 'ferric' and 'ferrous' contributions with δ = 0.39 mm/s, $|\Delta E_Q|$ = 1.15 mm/s (51 %) and δ = 0.53 mm/s, $|\Delta E_Q|$ = 3.24 mm/s (49 %). Summation of both lines affords the red line.
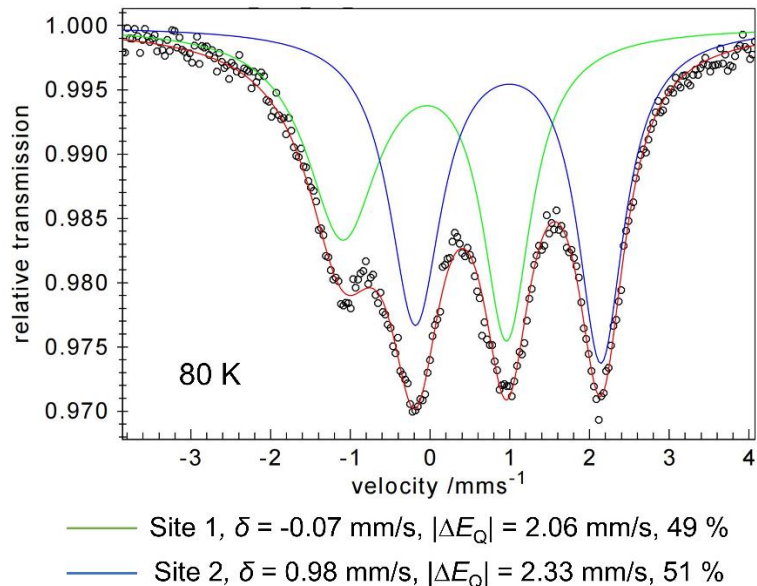
Figure S19. Zero-field ^{57}Fe Mössbauer spectrum of [Fe$_2$(μ-S)$_2$(ICy)$_4$][BPh$_4$] (**2**) measured at 80 K with a different simulation. Green and blue sub-spectra are fitted to the contributions of two sites with δ = -0.07 mm/s, $|\Delta E_Q|$ = 2.06 mm/s (49 %) and δ = 0.98 mm/s, $|\Delta E_Q|$ = 2.33 mm/s (51 %). Summation of both lines affords the red line.

Orbital	UNO 292	UNO 293	UNO 294	UNO 295	UNO 296
Occupation Number	1.99	1.43	1.34	1.21	1.07

Orbital	UNO 297	UNO 298	UNO 299	UNO 300	UNO 301
Occupation Number	1.00	0.93	0.79	0.66	0.57

Figure S20. Selected unrestricted natural orbitals (UNOs) of $[Fe_2(\mu\text{-}S)_2(ICy)_4][BPh_4]$ (**2**) in the antiferromagnetic spin state ($S = 1/2$).

Figure S21. Mulliken spin density population of $[Fe_2(\mu\text{-}S)_2(ICy)_4][BPh_4]$ (**2**) for its $S = 1/2$ state.

UNO 297
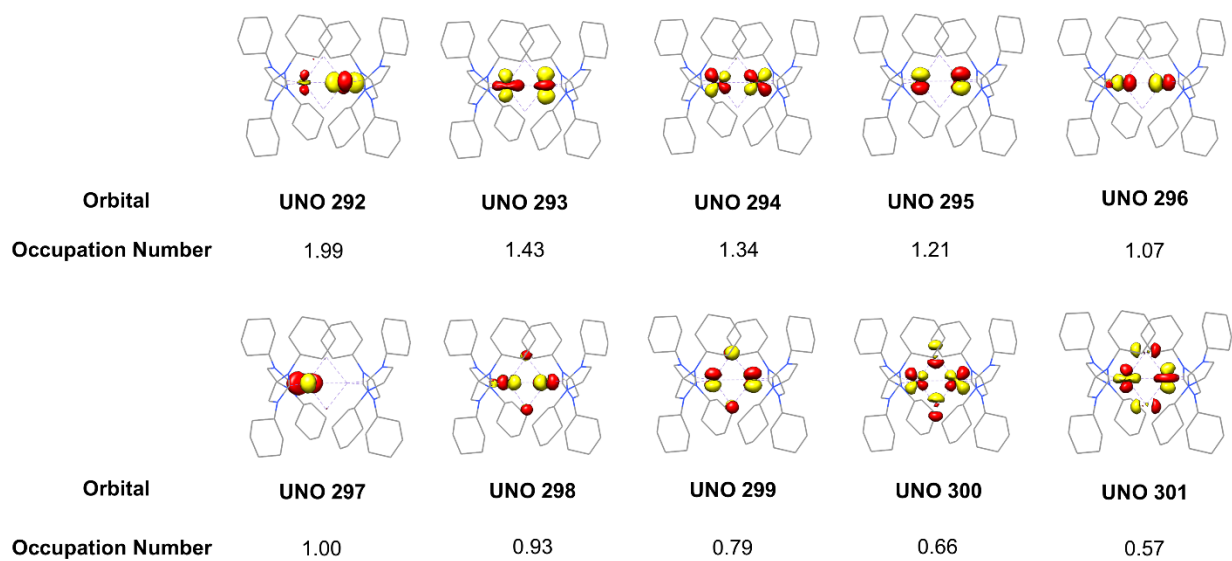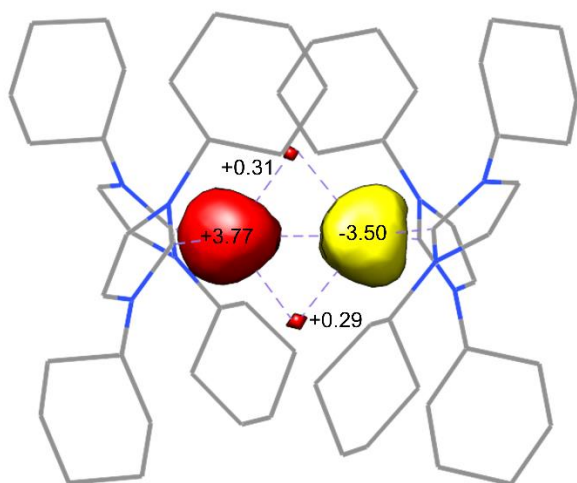Fe1 3*d* 87.2%
S1 2*p* 1.6%
S2 2*p* 1.5%

UCO 296α
Fe1 3*d* 72.7%
S1 2*p* 5.3%
S2 2*p* 5.7%

$S_{\alpha\beta} = 0.07$

UCO 296β
Fe2 3*d* 83.4%
S1 2*p* 1.5%
S2 2*p* 1.7%

UCO 295α
Fe1 3*d* 78.9%
Fe2 3*d* 3.1%
S1 2*p* 8.3%
S2 2*p* 6.9%

$S_{\alpha\beta} = 0.21$

UCO 295β
Fe1 3*d* 2.7%
Fe2 3*d* 92.8%
S1 2*p* 1.2%
S2 2*p* 1.0%

UCO 294α
Fe1 3*d* 66.5%
Fe2 3*d* 4.5%
S1 2*p* 9.7%
S2 2*p* 9.5%

$S_{\alpha\beta} = 0.33$

UCO 294β
Fe1 3*d* 5.3%
Fe2 3*d* 82.4%
S1 2*p* 2.6%
S2 2*p* 2.7%

UCO 293α
Fe1 3*d* 72.5%
Fe2 3*d* 8.6%
S1 2*p* 5.2%
S2 2*p* 5.3%

$S_{\alpha\beta} = 0.43$

UCO 293β
Fe1 3*d* 8.0%
Fe2 3*d* 79.8%
S1 2*p* 1.2%
S2 2*p* 1.1%
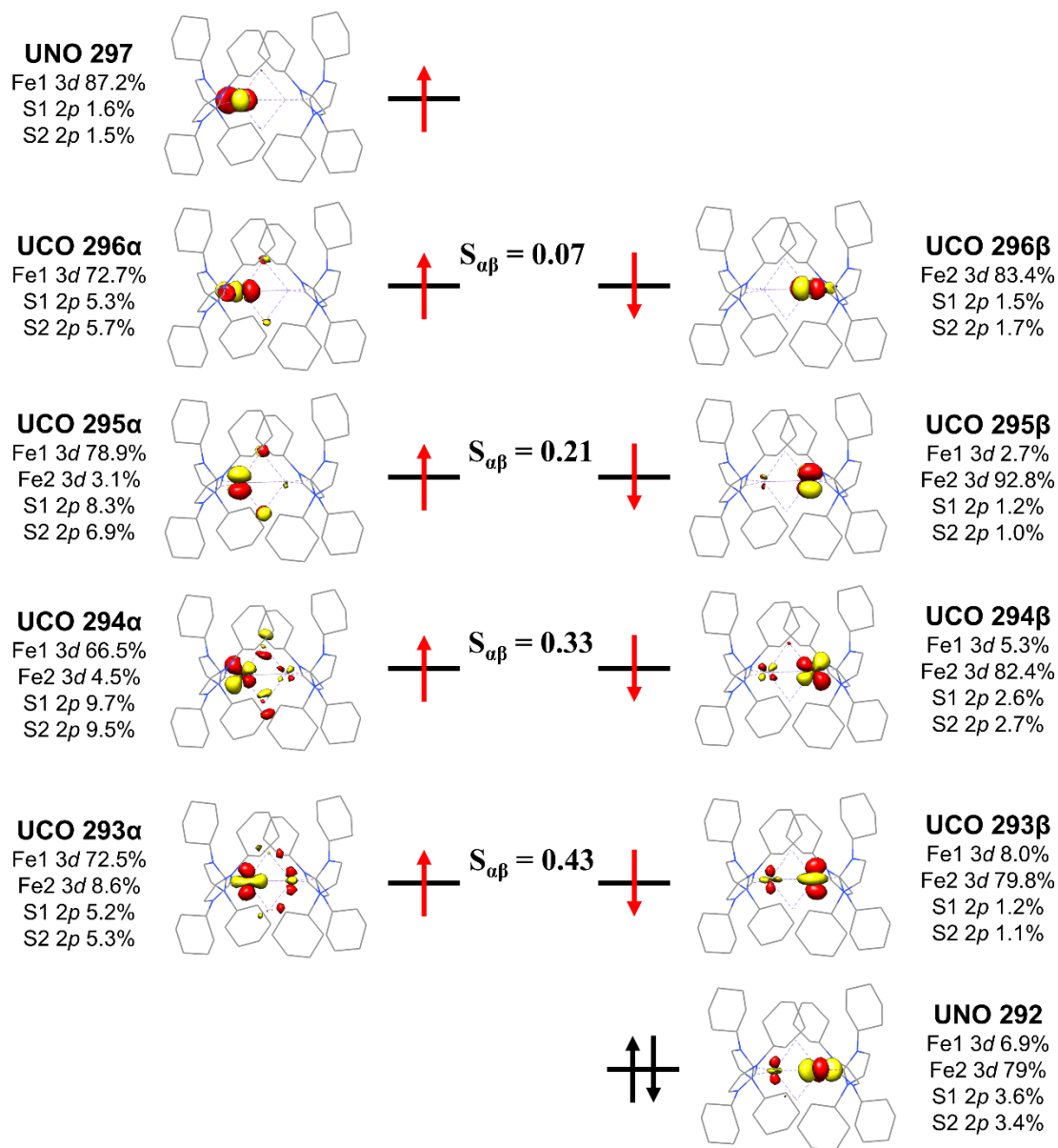
UNO 292
Fe1 3*d* 6.9%
Fe2 3*d* 79%
S1 2*p* 3.6%
S2 2*p* 3.4%

Figure S22. Selected unrestricted natural orbitals (UNOs) and unrestricted corresponding orbitals (UCOs) of [Fe$_2$(μ-S)$_2$(ICy)$_4$][BPh$_4$] (**2**) in the antiferromagnetic spin state ($S = 1/2$).

References

1. J. Rao, S. Dong, C. Yang, Q. Liu, X. Leng, D. Wang, J. Zhu and L. Deng, A triplet iron carbyne complex, *J. Am. Chem. Soc.*, 2023, **145**, 25766-25775.

2. L. Tendera, M. S. Luff, I. Krummenacher and U. Radius, Cationic nickel d^9-metalloradicals $[Ni(NHC)_2]^+$, *Eur. J. Inorg. Chem.*, 2022, **31**, e202200416.

3. H. Zhang, Z. Ouyang, Y. Liu, Q. Zhang, L. Wang and L. Deng, (Aminocarbene)(divinyltetramethyldisiloxane)Iron(0) compounds: a class of low-coordinate iron(0) reagents, *Angew. Chem. Int. Ed.*, 2014, **53**, 8432-8436.

4. M. Scholl, T. M. Trnka, J. P. Morgan and R. H. Grubbs, Increased ring closing metathesis activity of ruthenium-based olefin metathesis catalysts coordinated with imidazolin-2-ylidene ligands, *Tetrahedron*, 1999, **55**, 14523-14534.

5. Burling, B. M. Paine, D. Nama, V. S. Brown, M. F. Mahon, T. J. Prior, P. S. Pregosin, M. K. Whittlesey and J. M. J. Williams, C-H activation reactions of ruthenium N-heterocyclic carbene complexes: application in a catalytic tandem reaction involving C-C bond formation from alcohols, *J. Am. Chem. Soc.*, 2007, **129**, 1987-1995.

6. S. K. Sur, measurement of magnetic susceptibility and magnetic moment of paramagnetic molecules in solution by high-field fourier transform NMR spectroscopy, *J. Magn. Reson.*, 1989, **82**, 169-173.

7. D. F. Evans, The determination of the paramagnetic susceptibility of substances in solution by nuclear magnetic resonance, *J. Chem. Soc.*, 1959, **0**, 2003-2005.

8. S. Stoll and A. Schweiger, EasySpin, a comprehensive software package for spectral simulation and analysis in EPR, *J. Magn. Reson.*, 2006, **178**, 42–55.

9. Available from E.B.: http://ewww.mpi-muelheim.mpg.de/bac/logins/bill/julX_en.php.

10. G. M. Sheldrick, *SADABS, Program for Empirical Absorption Correction of Area Detector Data*, University of Göttingen, Germany, 1996.

11. G. M. Sheldrick, *SHELXTL 5.10 for Windows NT: Structure Determination Software Programs*, Bruker Analytical X-ray Systems, Inc., Madison, WI, 1997.

12. P. Hohenberg. and W. Kohn, Inhomogeneous Electron Gas, *Phys. Rev. B*, 1964, **136**, 864-871.

13. F. Neese, The ORCA program system, *WIREs Comput Mol Sci*, 2012, **2**, 73-78.

14. F. Neese, Software update: The ORCA program system — version 5.0, *WIREs Comput Mol Sci*, 2022, **12**, e1606.

15. A. D. Becke, Density-Functional thermochemistry. III. the role of exact exchange, *J. Chem. Phys.*, 1993, **98**, 5648-5652.

16. C. Lee, W. Yang and R. G. Parr, Development of the Colle-Salvetti correlation-energy formula into a functional of the electron density, *Phys. Rev. B*, 1988, **37**, 785-789.

17. M. Reiher, Relativistic Douglas-Kroll-Hess theory, *Wiley Interdiscip. Rev. Comput. Mol. Sci.*, 2012, **2**, 139–149.

18. D. A. Pantazis, X.-Y. Chen, C. R. Landis and F. Neese, All-electron scalar relativistic basis sets for third-row transition metal atoms, *J. Chem. Theory Comput.*, 2008, **4**, 908-919.

19. F. Weigend, Accurate coulomb-fitting basis sets for H to Rn, *Phys. Chem. Chem. Phys.*, 2006, **8**, 1057–1065.

20. F. Neese, F. Wennmohs, A. Hansen and U. Becker, Efficient, approximate and parallel Hartree-Fock and hybrid DFT calculations. A "chain-of-Spheres" algorithm for the Hartree-Fock exchange, *Chem. Phys.*, 2009, **356**, 98–109.

21. S. Grimme, S. Ehrlich and L. Goerigk, Effect of the damping function in dispersion corrected density functional theory, *J. Comput. Chem.*, 2011, **32**, 1456–1465.

22. S. Grimme, J. Antony, S. Ehrlich and H. Krieg, A consistent and accurate Ab initio parametrization of density functional dispersion correction (DFT-D) for the 94 elements H-Pu, *J. Chem. Phys.*, 2010, **132**, 154104-154122.

23. F. Neese, Prediction and interpretation of the 57Fe isomer shift in Mössbauer spectra by density functional theory, *Inorg. Chim. Acta.*, 2002, **337**, 181-192.

24. M. Römelt, S. Ye and F. Neese, Calibration of modern density functional theory methods for the prediction of 57Fe Mössbauer isomer shifts: Meta-GGA and Double-Hybrid functionals, *Inorg. Chem.*, 2009, **48**, 784-785.

25. K. Yamaguchi, Y. Takahara and T. Fueno, *Ab-Initio Molecular Orbital Studies of Structure and Reactivity of Transition Metal-OXO Compounds*, Springer Netherlands, Dordrecht, 1986.

26. T. Soda, Y. Kitagawa, T. Onishi, Y. Takano, Y. Shigeta, H. Nagao, Y. Yoshioka and K. Yamaguchi, Ab initio computations of effective exchange integrals for H–H, H–He–H and Mn_2O_2 complex: comparison of broken-symmetry approaches, *Chem. Phys. Lett.*, 2000, **319**, 223-230.